Direct evidence of local photochemical production driven ozone

2 episode in Beijing: a case study

- 3 Zhaofeng Tan^{1,2,3,#}, Xuefei Ma^{1,3,#}, Keding Lu^{1,3,*}, Meiqing Jiang^{1,3}, Qi Zou^{1,3}, Haichao Wang^{1,3,a}, Limin
- 4 Zeng^{1,3}, Yuanhang Zhang^{1,3,4,*}
- ¹ State Key Joint Laboratory of Environmental Simulation and Pollution Control, College of Environmental
- 6 Sciences and Engineering, Peking University, Beijing, China
- 7 ² Institute of Energy and Climate Research, IEK-8: Troposphere, Forschungszentrum Juelich GmbH, Juelich,
- 8 Germany

1

- ⁹ International Joint laboratory for Regional pollution Control (IJRC), Peking University, Beijing, China
- ⁴ Beijing Innovation Center for Engineering Sciences and Advanced Technology, Peking University, 100871,
- 11 Beijing, China
- ^a now at: School of Atmospheric Sciences, Sun Yat-Sen University, Guangzhou, China
- 14

17

13

- # These authors contributed equally to this work.
- 16 Correspondence to: Y. Zhang (yhzhang@pku.edu.cn),;K.Lu (k.lu@pku.edu.cn)
- elucidate the photochemical smog pollution, i.e. Ozone (O₃). The observed daily maximum hydroxyl radical (OH) and hydroperoxy radical (HO₂) concentrations were up to 1×10⁷ cm⁻³ and 6×10⁸ cm⁻³, respectively, indicating the active photochemistry in autumn Beijing. Photolysis of nitrous acid (HONO)

Abstract: We present a comprehensive field campaign conducted in Beijing, September 2016, to

- 21 and O₃ contributed 1-2 ppbv h⁻¹ to OH primary production during daytime. OH termination were
- dominated by the reaction with nitric oxide (NO) and nitrogen dioxide (NO₂), which were in general
- 23 larger than primary production rates, indicating other primary radical sources maybe important. The
- 24 measurement of radicals facilitates the direct determination of local ozone production rate P(O_x)
- 25 (O_x=O₃+NO₂). The integrated P(O_x) reached 75 ppbv in afternoon (for 4 hours) when planetary
- boundary layer was well developed. At the same time period, the observed total oxidant concentrations
- O_x, increased significantly by 70 ppbv. In addition, the O_x measurement showed compact increase in 12

stations both temporally and spatially in Beijing, indicating that active photochemical production happened homogenously throughout the city. The back-trajectory analysis showed that Beijing was isolated from the other cities during the episode, which further proved that the fast ozone pollution was contributed by local photochemical production rather than regional advection.

Keyword: atmospheric radicals, ozone, local ozone production rate

Introduction

28

29

30

31

32

33

34

35

36

37

38

39

40

41

42

43

44

45

46

47

48

49

50

51

52

53

Air quality has been deteriorated for the past decades in China, especially in the fast-developed eastern regions. The capital Beijing has been experiencing severe air pollution, among which the winter haze characterized by high loads of fine particles is most well-known. Recent studies showed that secondary compounds are the major components of fine particles (Guo et al., 2014; Huang et al., 2014; Lei et al., 2021; Sun et al., 2014), indicating that oxidation processes play important role in particle formation. Ozone is also a secondary pollutant generated from photochemical processes. The most famous "Los Angeles-type" smog is characterized by hazardous level of ozone. Numerous scientific research and investigations focus on this issue have been taken since then. However, the ozone problem in Beijing is not well acknowledged. Actually, ozone is the only one out of six components of China's official air quality index that increases over the past several years despite the implementation of regional emission control. Ozone has become the major air pollutant in Beijing (Wang et al., 2017b; Zhang et al., 2014). Ozone is produced from the photochemical reactions between NO_x (the sum of nitric oxide (NO) and nitrogen dioxide (NO₂)) and volatile organic compounds (VOCs), both of which are emitted by anthropogenic activities (Cardelino and Chameides, 1995; Liu, 1977). However, the variation of ozone concentrations in a certain location is affected by both chemical (photochemical production, titration by NO) and physical (horizontal advection, vertical mixing, deposition and so on) processes. In urban environments, O_3 is titrated to NO_2 by fresh emitted NO. Therefore, O_x , the sum of O_3 and NO_2 , is a better metric to quantify the extent of ozone pollution in urban areas, because it is conservative and independent of fresh NO emission influence (Kleinman et al., 2002; Kley et al., 1994).

Specifically, the variation of O_x concentrations depends on the local production, vertical transport across layers, vertical deposition, and horizontal advection (E1).

$$\frac{d(O_x)}{d(t)} = P(O_3) + \frac{w_e \Delta O_x}{H} - \frac{v}{H} \left[O_x\right] + u_i \frac{\partial \left[O_x\right]}{\partial x_i}$$
(E1)

57

58

59

60

61

62

63

64

65

66

67

68

69

70

71

72

73

74

75

76

77

78

79

 $P(O_3)$ is the effective ozone production rate including both production and destruction terms (detail see below). Vertical transport across layers term consists of the entrainment velocity, w_e and the difference between upper and lower layers, $\triangle O_x$, and is scaled by the planetary boundary layer (PBL) height, H. The dry deposition is determined by the deposition velocity, v, the PBL height, H and the O_x concentrations in PBL, $[O_x]$. Horizontal advection depends on the wind velocity, u_i , and the O_x concentration gradient along the wind direction, $\frac{\partial [O_x]}{\partial x_i}$.

The direct determination of photochemical ozone production is limited due to lack of radical measurements. A few studies in large cities in other countries based on the measurements of radical concentrations or direct ozone production rates have shown that ozone production mechanism is not well described by the current chemical models for high NO_x conditions (Baier et al., 2015; Baier et al., 2017; Brune et al., 2016; Cazorla et al., 2012; Cazorla and Brune, 2010; Griffith et al., 2016; Kanaya et al., 2008; Thornton et al., 2002; Whalley et al., 2018). A previous summer field campaign with OH and HO₂ radical measurements at a suburban site in Beijing showed that P(O₃) reached 50 ppbv h⁻¹, which was higher than the increase in the ozone concentrations (Lu et al., 2010). A recent study in downtown Beijing also present high ozone production (Whalley et al., 2021). Long term measurements demonstrated that increasing O₃ trend in Beijing was due to active local photochemistry (Chen et al., 2020; Wang et al., 2020). However, another study using an observational based model found that the dramatic increase of O₃ was dominated by advection from a case study at a suburban site in Beijing (Xue et al., 2014). Nevertheless, the in-situ measurement of HO_x radical in Beijing is still sparse to determine the local ozone production and to understand the ozone formation mechanism in Beijing. Additionally, the ozone peak value observed in the surface was tightly related to the favorable meteorology, such as high temperature, strong sunlight, and stagnant air conditions (Ding et al., 2008; Li et al., 2020; Lu et al., 2019b), which indicates the importance of meteorological factors.

Autumn is a transition from summer photochemical pollution to winter particle haze. The combination of active photochemistry and poor pollution advection could result in severer photochemical smog. To elucidate the ozone pollution formation mechanism in autumn Beijing, we conducted a field campaign with OH and HO₂ radical measurements at an urban site in Beijing in 2016 from September to October. The observed concentrations of OH and HO₂ radicals, as well as other parameters, enable to calculate the local photochemical production rates of ozone and further reveal the formation of ozone pollution in Beijing for a typical episode. This field campaign in Beijing provides experimental data to interpret the ozone formation mechanism in this transition season.

Methodology

80

81

82

83

84

85

86

87

88

89

90

91

92

93

94

95

96

97

98

99

100

101

102

103

104

105

106

Measurement site and instrumentation

The campaign was conducted on the campus of Peking University (39.99°N, 116.30° E) in the northwest of the Beijing city center (Fig. 1) from August 30 to October 4, 2016. It represents a typical urban environment characterized by strong anthropogenic emissions. All measurements were taken on the roof of a building (approximately 20 m above the ground), and the instruments inlets were 1.7 m above the roof. The measurements included the concentrations of trace gas compounds and the properties of particles. Details of the instrumentation setup deployed can be found in a previous publication (Wang et al., 2017a). OH radical concentrations measurements were performed by a Laser-Induced Fluorescence (LIF) system, which has been successfully deployed in both winter and summer campaigns, and the details have been described by Tan et al. (2017). HO₂ was converted to OH in the measurement cell by adding 5 ppm NO. The added NO mixing ratio was chosen in a low range to minimize the RO₂ interreference, resulting in the maximum HO₂ conversion efficiency to be 20%. The detection limit was 0.5×10^6 cm⁻³ for OH and 0.3×10^8 cm⁻³ for HO₂ (1 σ), and the uncertainty of OH and HO₂ measurements were estimated to be 12% and 16%, respectively. O₃, NO, NO₂ and CO were detected by a series of commercial analyzers from Thermo Inc. O₃ was measured by a UV Photometric analyzer (Model 49i). NO and NO2 were measured by a trace-level analyzer (Model 42i) using chemiluminescence method. HONO was measured by a home-built Long-path Absorption Photometry, which was shut down on September 10 due to technical failure. Photolysis frequencies were calculated from the spectral actinic photon flux density measured by a spectroradiometer (Bohn et al., 2008). Meteorological parameters including temperature, relative humidity, pressure, wind speed, and wind direction were measured on site.



Figure 1. The map of North China Plain and the PKU site location.

OH radical budget analysis

The OH radical reactions can be classified into three groups, namely initiation, termination, and propagation (including conversion from OH to HO₂ and organic peroxy radical (RO₂), and the OH regeneration from HO₂). The involved radical reactions are summarized in Table S1 and explained in supplement for the specific conditions during this campaign. The OH initiation also known as radical primary source consists of (1) photolysis of HONO, (2) photolysis of O₃ followed by H₂O addition, and (3) ozonolysis of alkenes. Due to the limitation of measured parameters, we can only quantify the first two terms.

OH termination includes the reactions with NO and NO₂ producing HONO and HNO₃ (nitric acid). The reaction between OH and NO is the counteract reaction of HONO photolysis, which compensates the significance of HONO photolysis. On the other hand, the NO₂ oxidation rate by OH radical can be considered as the production rate of nitric acid, an important precursor for particulate nitrate.

OH is converted to HO_2 and RO_2 via the reactions with CO, HCHO, and other VOCs. The produced peroxy radicals can loss to non-radical species (see supplement), or regenerate OH radical with sufficient NO, which is the only known reaction producing ozone from atmospheric chemistry in troposphere.

Determination of local total oxidant production rate $P(O_3)$

The net photochemical ozone production rate P(O₃) can be determined by the difference between gross formation rate F(O₃) and loss rate D(O₃) (E2). All the involved reactions are summarized in Table S2. The ozone formation rate is calcualted from the NO oxidation rate by HO₂ and RO₂ (E3). We assume the HO₂ and RO₂ concentrations are the same to calculate P(O₃) since only HO₂ concentrations were measured during this campaign. This assumption is justified in high NO_x conditions (Martinez et al., 2003; Mihelcic et al., 2003; Slater et al., 2020; Tan et al., 2018c; Whalley et al., 2021), because the efficient RO₂ conversion to HO₂ reconciles the HO₂ concentration to the RO₂ concentrations. Also, the difference in reaction rates of HO₂ and RO₂ with NO is less than 10%. The F(O₃) is thus estimated to be two-folds of reaction rate of HO₂ and NO. The threshold of low- and high-NO_x conditions is determined by the relative importance of the radical termination through reaction with NO and peroxy radical self-combination (see supplement) which is calculated to be 2 ppbv during this campaign. This value is usually below the typical NO_x concentration encountered indicating a persistent high-NO_x condition during this campaign.

141
$$P(O_3) = F(O_3) - L(O_3)$$
 (E2)

142
$$F(O_3) = k_{HO_2+NO} [HO_2] [NO] + \sum k_{RO_2+NO} [RO_2] [NO] = 2 \times k_{HO_2+NO} [HO_2] [NO]$$
 (E3)

The chemical loss of ozone includes photolysis and reactions with alkenes, OH, and HO_2 . In addition, the reaction of NO_2 with OH is also a chemical loss of O_x because NO_2 is converted to HNO_3 before photolysis to generate ozone. The O_x loss is dominated by the $OH+NO_2$ reaction contributing on average 83% to the total O_x loss during this campaign because of the high NO_x concentratoins.

147
$$L(O_3) = k_{OH+NO_2} [OH] [NO_2] + f_{H_2O} j(O^1D) [O_3] + k_{O_3+OH} [O_3] [OH] + k_{O_3+HO_2} [O_3] [HO_2]$$
 (E4)

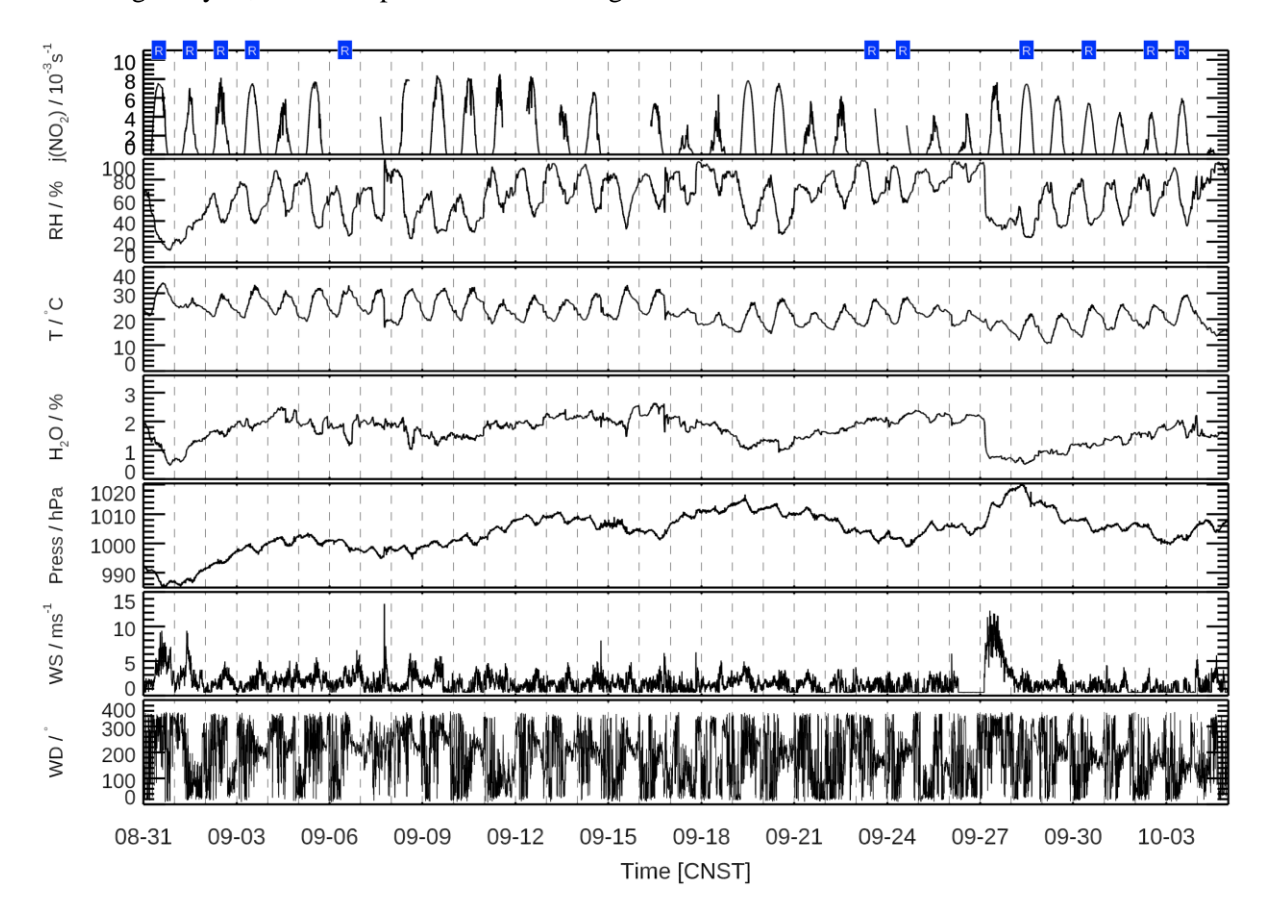
Results and discussion

Overview of measurements

The measured meteorological parameters and trace gases concentrations are shown in Fig. 2. The daily ambient temperature maximum was above 30 degrees Celsius at the beginning of the campaign and dropped to between 25 and 30 degrees Celsius at the end. In general, the wind speed was usually 2-

3 m s⁻¹. The wind direction typically switched from north in the morning to south in the afternoon (Fig. S2).

CO is a tracer for anthropogenic pollution, more in regional scale due to its long lifetime. There were approximately four large episodic increases in CO during the measurement period (Fig.S1). In contrast, NO_x concentrations increase is more related to local emission due to its short lifetime. The NO_x concentrations showed typical diurnal profiles with maximum in the morning rush hours due to traffic emission. However, the regional scale pollution is not necessary for local photochemical smog. In the following analysis, we found photochemical smog occurred in different circumstances.



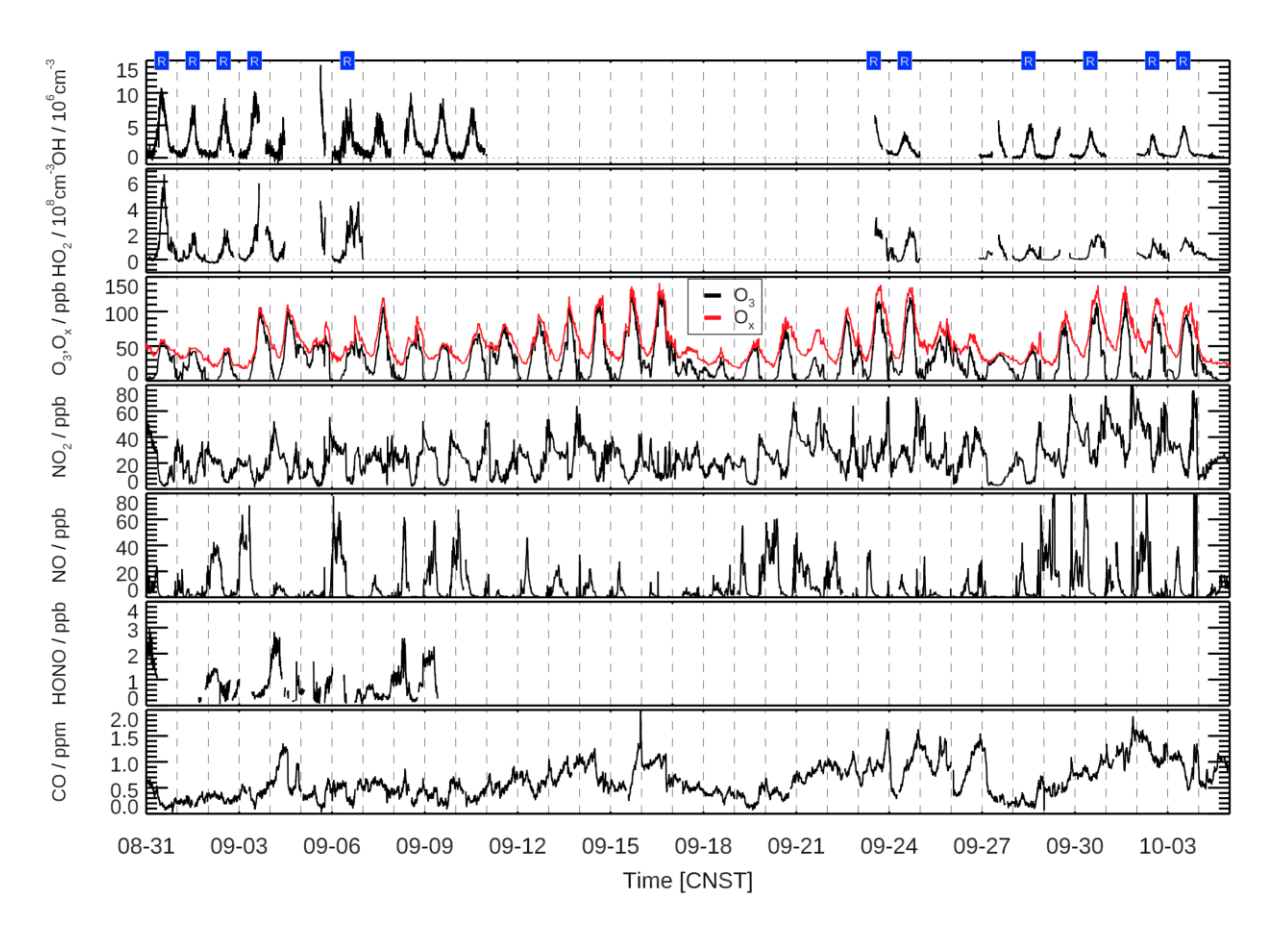


Figure 2. Time series of measured parameters over the whole campaign. The label 'R' on top of the figure denotes the date when both OH and HO_2 radical measurements were available during the afternoon (12:00 to 16:00).

 O_3 concentrations showed typical diurnal profiles with maxima in the afternoon due to photochemical reactions. The maximum O_3 concentrations were more than 100 ppbv during a few episodes (Fig. 2). It is worth noting that O_3 can be titrated by fresh emitted NO and converted to NO_2 . In this case, O_3 was stored in the form of NO_2 and regenerated by photolysis. Hence, O_x , the sum of NO_2 and O_3 , are usually used to illustrate the ozone pollution in urban area, which are more conservative than O_3 . The O_x concentrations reached 130 ppbv in a few periods (Fig. 2). In addition, the photochemical smog characterized with high O_x concentrations, mainly happened in the south wind sector with lower wind speed (Fig. S1).

The radical measurements were available from 31 August to 5 September and from 26 September to 5 October (Fig. 2). The data gap was caused by the LIF instrument failure. Observed OH concentrations showed distinct diurnal variations, with daily peak values ranging from 3×10^6 cm⁻³ to

1×10⁷ cm⁻³. The lower OH concentrations was observed on cloudy days while the high range of observed OH concentrations were comparable to what has been observed in summer in other urban areas (Griffith et al., 2016; Kanaya et al., 2007; Michoud et al., 2012; Ren et al., 2013; Shirley et al., 2006; Whalley et al., 2018). A recent campaign conducted in Beijing during summer observed OH concentrations reaching up to 2.8×10⁷ cm⁻³ with a diurnal averaged maximum of 8×10⁶ cm⁻³ (Whalley et al., 2020). For comparison, the diurnal averaged maximum was 4.5×10⁶ cm⁻³ in a field campaign in Pearl River Delta, in China during autumn (Tan et al., 2019). The relatively high OH concentration during autumn, which is sustained by the high level of radical precursors, e.g. HONO and HCHO suggests active photochemistry persists from summer to autumn, at least for two representative populated areas in China. In winter, the measured OH concentration drops to 2-3×10⁶ cm⁻³ for diurnal averaged maximum (Lu et al., 2019a; Ma et al., 2019; Slater et al., 2020; Tan et al., 2018c). Besides, during this autumn campaign, the daily maximum of HO₂ concentrations varied from 1×10⁸ cm⁻³ to 6×10⁸ cm⁻³. The following discussion will focus on one episode (September 1-3) to elucidate the radical chemistry and ozone pollution formation as well as their relationship.

Radical concentrations and budget analysis

Successive radical measurements were performed from Aug. 31 to Sep. 3. A data gap for radical measurements from 15:50 to 19:40 on Sep.3 was due to instrument maintenance (Fig. 2). The missing radical concentrations were interpolated linearly over the data gap to calculate the turnover rate as discussed below. O_x concentrations increased from 40 ppbv at 12:00 to 110 ppbv at 16:00 on Sep. 3 (Fig. S2). At the same time, observed HO_2 concentrations increased continuously from 2×10^8 cm⁻³ to 6×10^8 cm⁻³ and maintained at 2×10^8 cm⁻³ after sunset (Fig. 2). The maximum OH concentrations reached 1×10^7 cm⁻³ at noontime (Fig. 2), indicating photochemical processes were active. The following analysis focus on the radical measurement and budget to illustrate the key process of radical reaction during this period (Fig. 3).

Using the measured radical concentrations, one could determine the turnover rates of a few key reactions and further perform radical budget analysis. OH radicals were initially produced from the HONO photolysis and the reaction between O¹D (generated in O₃ photolysis) and H₂O, which were in the range of 1-2 ppbv h⁻¹ during daytime (Fig. 3a). The OH radical termination processes include

reactions with NO and NO₂ producing HONO and HNO₃ (Fig. 3b). The NO reaction path showed steep morning peak up to about 4 ppbv h⁻¹ on Sep. 2 and 3. The NO₂ reaction path showed similar morning peak on Sep. 2 with a longer tailing. While the OH+NO₂ reaction showed a peak at 14:00 on Sep. 3, coinciding with a NO₂ peak being 15 ppbv (Fig. S2). The large radical turnover rate could not be attributed to the data gap of radical measurement which did not appear until 15:50. As shown in Fig. 3c, the OH termination rates (OH reaction with NO and NO₂) are in general larger than OH primary production rates (HONO photolysis and O₃ photolysis), which suggests additional primary radical source plays a role in the radical chemistry. For example, the alkene ozonolysis reaction and the photolysis of carbonyl species were not considered in this study due to lack of VOC measurements. Besides, missing RO₂ primary sources were found in a rural site (Wangdu) in North China Plain during summer (Tan et al., 2017) and in a suburban site (Huairou) in Beijing during winter (Tan et al., 2018a). Summer and winter field campaigns at an urban site in Beijing also found significant missing radical source (Slater et al., 2020; Whalley et al., 2020). These results highlight the importance of missing radical source contributing to strong local ozone production in Beijing. In this study, the unknown radical source could not be quantified due to the lack of measurement for other parameters, but the local ozone production is determined directly using radical measurements. On Sep. 3, the OH termination rate remained at the range of 1-2 ppbv h⁻¹ after 19:40 (sunset at about 18:00), indicating non-photolytic sources producing radicals.

206

207

208

209

210

211

212

213

214

215

216

217

218

219

220

221

222

223

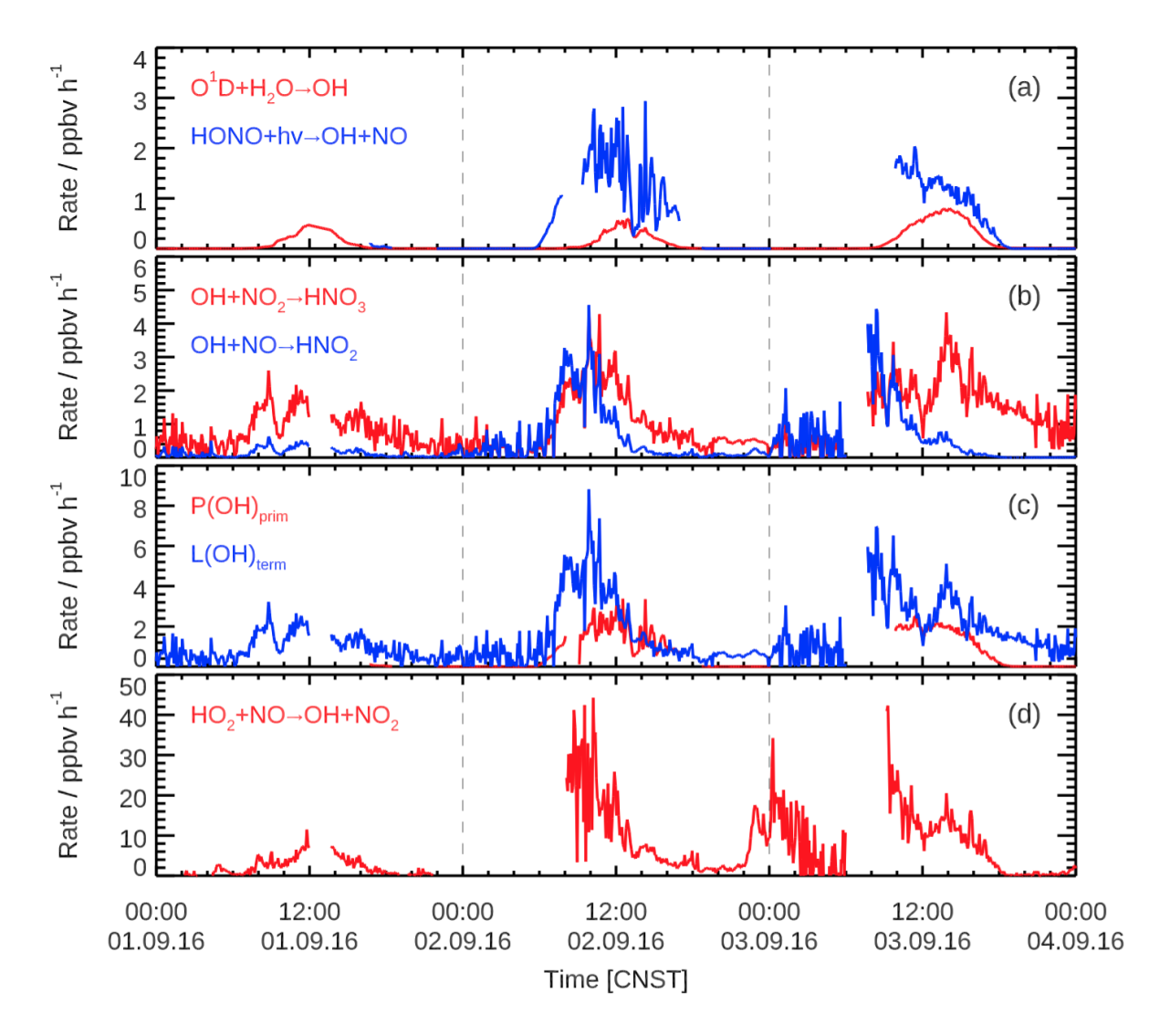


Figure 3. Time series of experimental determined reaction turnover rates, including (a) the OH production from O₃ photolysis and HONO photolysis; (b) the OH termination via reactions with NO and NO₂; (c) the calculated OH budget (see text) and (d) OH regeneration from HO₂ via NO reactions.

The reaction to reform OH radical is more important with respective to ozone pollution. OH radical is regenerated from HO₂ and NO reaction, which oxidize NO to NO₂. The turnover rate from HO₂ to OH peaked in the morning exceeding 30 ppbv h⁻¹ on 2 and 3 September (Fig. 3d). The unique afternoon peak also appeared in the OH regeneration similar to the OH termination on Sep. 3 (Fig. 3c). The enhanced radical turnover rate on Sep. 3 during afternoon was unlikely attributed to measurement artifacts because these two reactions involve four different measured parameters. Besides, the elevated

OH recycling and termination rates while OH primary source was comparable to Sep. 2 suggest the enhanced photochemistry could be driven by other radical source(s).

The OH loss includes the termination reactions and the conversion to HO₂ and RO₂ by reacting with CO, HCHO and other VOCs. Given the termination is a minor part of the OH loss, the major OH loss is by reaction with CO and VOCs forming HO₂ and RO₂, which later on recycle to OH via NO reactions and resulting in ozone production in the meantime (see below).

By performing OH radical budget analysis, the daytime averaged VOC reactivity is estimated to be about 5.4 s⁻¹, which is consistent to previous studies in Beijing that the measured VOC reactivity ranges from 12 s⁻¹ in summer (Whalley et al., 2021) and 5.5 s⁻¹ in winter (Ma et al., 2019).

Relation between P(O₃) and O_x concentration

235

236

237

238

239

240

241

242

243

244

245

246

247

248

249

250

251

252

253

254

255

256

257

258

259

260

261

262

In this study, we analyzed the relationship between local ozone production and the variation of O_x concentrations using radical measurement during the afternoon hours. The PBL was well mixed and maintained at relatively constant height in the afternoon. The relative change of the bounder layer height was less than 10% (Fig, S3). Thus, the ozone entrainment from free troposphere was relatively small due to this small change rate between the mixing layer and free troposphere. In contrast, the PBL was only a few hundred meters in the early morning and increased sharply to 2 km at noon (Fig. S3). Therefore, the vertical transport was important due to the fast entrainment. In the morning, the upper layer is known as the residual layer (RL), which is isolated from the surface due to inversion at night. It is difficult to evaluate the impact of air entrainment from RL on the O_x abundance in the boundary layer due to the following facts. First, RL usually contains the air mass with higher O₃ concentration than that of nocturnal boundary layer. Second, the radical chemistry could be attenuated in RL because HONO concentration presents negative vertical gradient and its photolysis is the dominant radical source in the morning (Kim et al., 2014; Young et al., 2012), while ClNO₂ shows relatively constant concentrations along the altitude up to a few hundred meters (Riedel et al., 2013; Young et al., 2012), whose photolysis is also an important radical source in the morning and thus affecting ozone production. Therefore, the difference between two layers is indiscernible without supporting measurements, which make it difficult to estimate the effective ozone production from the radical measurement in the PBL and compare with the O_x concentration increase in the morning.

During afternoon, the PBL can be treated as a column to evaluate the ozone production by the insitu radical observation. The ozone production can be compared to the O_x concentration increase easily without the complexity in the vertical mixing for several hours during each afternoon (i.e. from 12:00 to 16:00). Besides, the time scale of vertical deposition of O_x is in the order of one day, at least one order of magnitude larger than that of chemical production. Therefore, the ozone budget in (E1) can be simplified by removing the vertical mixing and deposition terms (E5).

269
$$\frac{d(O_x)}{d(t)} = P(O_3) + u_i \frac{\partial [O_x]}{\partial x_i}$$
 (E5)

The impact on O_x concentrations due to vertical entrainment become negative because the O_x concentration is lower in the free troposphere than in the surface layer during afternoon (Kaser et al., 2017). In this study, the simplification of vertical entrainment in (E5) should be considered as an upper limit to estimate the O_x concentration change during the afternoon.

As shown in Fig. 4b, $P(O_3)$ determined according to E2 to E4 was integrated from 12:00 to 16:00 on each day. The integrated $P(O_3)$ was more than 40 ppbv and reached 75 ppbv on the last day, indicating active photochemical production. The $P(O_3)$ integration started at 12:00 using the noontime O_x concentrations as offset so that it can compared to the O_x concentration directly. The comparison is valid, if horizontal advection is negligible as denoted by (E5). However, if air mass exchanges efficiently and thus the horizontal advection become significant, the locally produced ozone cannot accumulate and thus has minor impact on O_x concentration. The O_x concentration increased following tightly the integrated $P(O_3)$ on September 3, indicating local photochemical production can support the fast O_x increase (70 ppbv in 4 hours). Meanwhile, only small O_x increase occurred on the other two days which could be explained by fast air mass exchange. To denote the horizontal air advection effect, O_x is assumed to be flushed out in 2 hours (estimated from the typical wind velocity of 5 m s⁻¹ and the radius of Beijing urban area of 40 km, and by using a dilution term equivalent to lifetime of 2 hours). The O_x concentration showed consistent trend with integrated $P(O_3)$ if fast air exchange was applied (Fig. 4b). Actually, most of the locally produced O_x (> 90%) was flushed out and transported to the downwind regions on these two days.

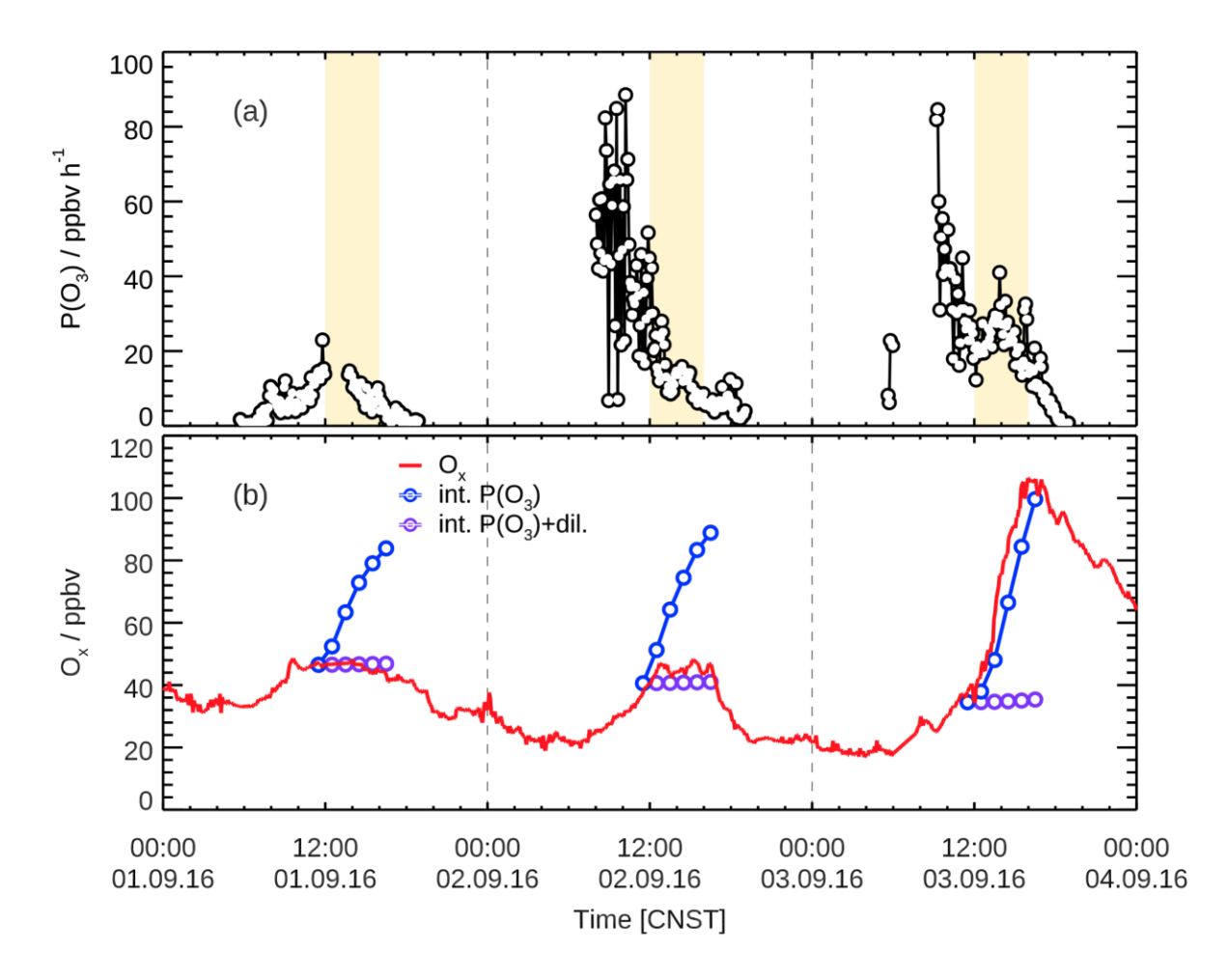


Figure 4. In-situ ozone budget analysis. (a) The time series of local ozone production rate that determined from the reaction rate between HO_2 and NO with a scaling factor of 2 to represent the sum of HO_2 and RO_2 (assuming similar contribution from HO_2 and RO_2) and corrected for the O_x loss rate via chemical reactions (Table S2). The yellow shaded areas denote the time window from 12:00 to 16:00. (b) The comparison of O_x concentrations and integrated $P(O_3)$ from 12:00 to 16:00. The integrated $P(O_3)$ is calculated in two scenarios that without additional loss (blue circles) and with a loss process in a time scale of 2 hours (purple circles, detail see text).

We also preformed back-trajectory analysis to investigate the meteorological conditions using the HYSPLIT model (Stein et al., 2015). The HYSPLIT model was operated in backward mode for 24 hours before the air masses arriving at the PKU site to track the origin of them. As shown in Fig. 5, the air masses were mainly originated from the north on both September 2 and 3. On the other hand, the forward mode shows that the airmasses left the city in 2 hours (not shown here). It indicates the air masses arived at Beijing were uncontaminated continental background air and then mixed with the local emission. However, the back-trajectory shows the air masses from the north first travel to the south part of Beijing

(30 km south of Tiananmen Square) and then circled back to the measurement site since 10:00 CNST on September 3 (Fig. S4). This results in a long residence time of the air parcel travelling in the urban area to accumulate the anthropogenic emission and photochemical products. The unique air mass trajectory facilitated to reserve the air parcel within Beijing and thus link the photochemical ozone production to O_x concentration increases. In addition, we found that Beijing was isolated from the cities to its south during the fast O_x increase period as denoted by the back-trajectory analysis (Fig. 5). Therefore, it is unlikely that O_x increase was related to regional advection. An evidence to support this argument is that O_x started to decrease shortly after sunset, which indicated the daytime O_x was sustained by photochemical production. These findings suggested that large $P(O_3)$ does not necessarily result in O_x increase, but should coincide with the meteorological field that constrains the local production within Beijing to lead to O_x increase.

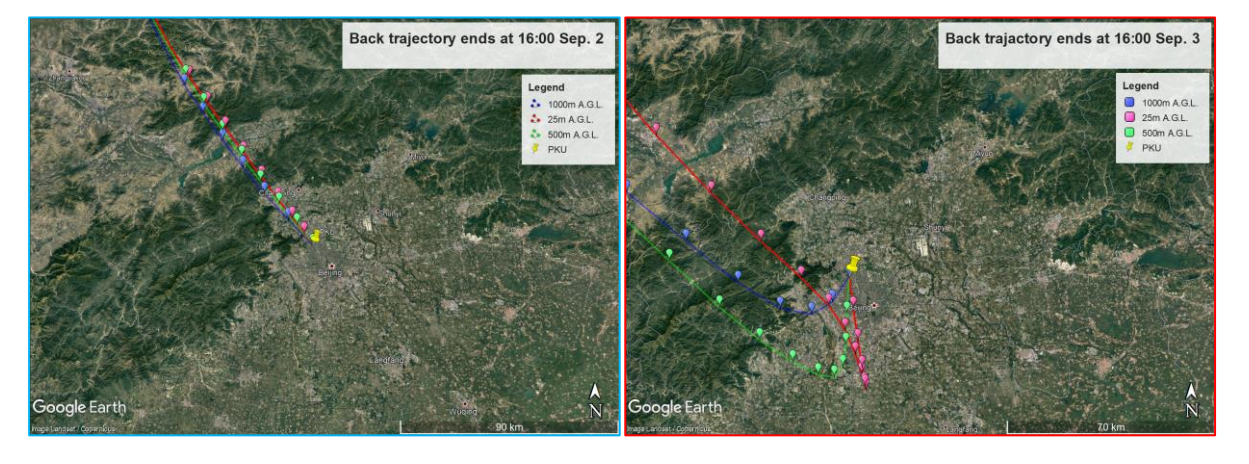


Figure 5. Back-trajectory analysis for the measurement site PKU on September 2 (left) and 3 (right) at 16:00. The back trajectory was simulated for three heights at PKU site. The stamps on the trajectory lines denote the hourly movement of air mass.

Based on this concept, we selected days characterized by both strong local ozone production and long residence time within Beijing during this campaign to compare the integrated ozone production with the observed O_x concentrations increases for the ozone pollution days in the afternoon (Fig. 6). 6 out of 12 days with HO_x radical measurement showed that local ozone production showed consistent trend with the O_x concentrations increases (20-70 ppbv in 4 hours). The severe ozone pollution episode

should result from a combination of active local photochemistry and appropriate meteorological conditions.

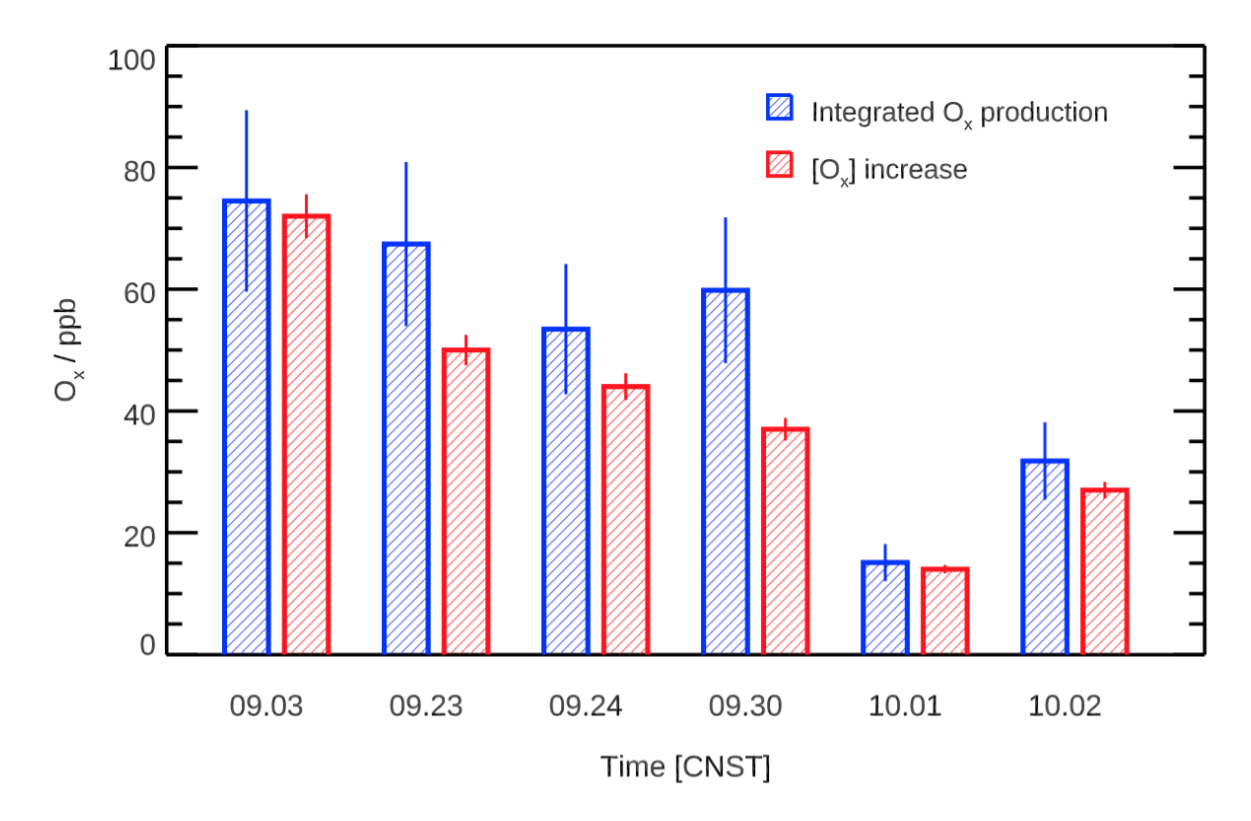


Figure 6. The comparison of integrated local ozone production rate (see Fig. 4, and no dilution) and O_x concentration increase from 12:00 to 16:00. The results are filtered for ozone pollution episodes (Sep. 3, 23, 24 and 30 and Oct. 1 and 2). The error bars denote the uncertainty of experimental determined parameters ($P(O_3)$: $\pm 20\%$, $\Delta(O_x)$: $\pm 5\%$,).

Furthermore, we compared the O_x concentrations at the PKU site to those observed at other 12 EPA stations in Beijing. All stations showed similar and compact O_x increases on September 3 (Fig. S6). Such fast O_x concentrations increases over whole Beijing demonstrated that Beijing is rather homogeneous and driven by active photochemistry. First, the compact O_x increase was unlikely caused by regional advection, because O_x concentrations increase would have shown a time shift between different stations if regional advection was the main force for O_x pollution. Second, the fast ozone increase happened in the afternoon period, when PBL was well developed. Hence, vertical entrainment was unlikely the cause of such fast ozone increase. Therefore, the O_x increase was most likely driven by local photochemical production. It is worth noting that the ozone production rate is calculated using the

measured radical concentrations. Previous studies found that current chemical models underpredicts observed HO_2 concentrations under high NO_x conditions in urban regions (Griffith et al., 2016; Kanaya et al., 2007; Ma et al., 2019; Michoud et al., 2012; Ren et al., 2013; Shirley et al., 2006; Slater et al., 2020; Tan et al., 2018b; Whalley et al., 2020; Whalley et al., 2018). Therefore, model simulation based on similar chemical mechanism may not reproduce the high radical concentrations and thus fast ozone production. The fast ozone production determined by radical measurement at PKU site happened homogenously over the whole Beijing urban areas. In fact, a previous study reported that high ozone concentrations (up to 286 ppbv) was attributed to strong photochemical production in the outflow plume from Beijing city (Wang et al., 2006). The photochemical ozone production in the afternoon that enhances the ozone concentrations was also found in a study based on satellite observation (Cuesta et al., 2018).

Conclusion

In this study, we performed a detail analysis on an ozone pollution episode in autumn Beijing using the in-situ radical and long-lived trace gases measurements. The daily maximum OH concentrations were up to 1×10^7 cm⁻³, and the maximum of HO₂ ranged from 1×10^8 to 6×10^8 cm⁻³. OH radical primary production from HONO and O₃ photolysis were determined to be in the range of 1-2 ppbv h⁻¹ during daytime. OH termination rates via reaction with NO and NO₂ were in generally larger than primary production rates, indicating other primary radical sources, such as alkene ozonolysis reaction and the photolysis of carbonyl species, kick in radical chemistry. However, these processes were not considered in this study due to lack of related measurements.

During the pollution episodes, experimentally determined ozone production was sufficient to support the O_x concentrations increases. The largest integrated ozone production from 12:00 to 16:00 was found to be 75 ppbv on September 3, indicating extremely active photochemical processes. Combining the back-trajectory analysis, we found that both fast ozone production rate and long residence time within the city were necessary for O_x accumulation. The combination of in-situ radical measurement and regional air quality data provide experimental evidence that fast local photochemical ozone production contributes to ozone pollution in Beijing. Therefore, with similar meteorological

conditions to the investigated case, ozone pollution control in Beijing requires local emission mitigation while regional transportation has minor contribution.

Acknowledgments. The authors would like to thank the three anonymous reviewers for useful suggestions and comments. The authors also thank Dr. Franz Rohrer for valuable discussion. This work was supported by the National Natural Science Foundation of China (Grant No. 91544225, 21522701, 41375124), the National Science and Technology Support Program of China (No.2014BAC21B01), the Strategic Priority Research Program of the Chinese Academy of Sciences (grant No. XDB05010500), the special fund of State Environmental Protection Key Laboratory of Formation and Prevention of Urban Air Pollution Complex (grant No. CX2020080090). The authors would like to thank the China Ministry of Environmental Protection Ministry for the CO, O₃ and NO_x observations. The authors gratefully acknowledge the NOAA Air Resources Laboratory (ARL) for the provision of the HYSPLIT transport and dispersion model and READY website (http://www.ready.noaa.gov) used in this publication.

Reference

Baier BC, Brune WH, Lefer BL, Miller DO, Martins DK. Direct ozone production rate measurements and their use in assessing ozone source and receptor regions for Houston in 2013. Atmospheric Environment 2015; 114: 83-91.

Baier BC, Brune WH, Miller DO, Blake D, Long R, Wisthaler A, et al. Higher measured than modeled ozone production at increased NOx levels in the Colorado Front Range. Atmos. Chem. Phys. 2017; 17: 11273-11292.

Bohn B, Corlett G, Gillmann M, Sanghavi S, Stange G, Tensing E, et al. Photolysis frequency measurement techniques: results of a comparison within the ACCENT project. Atmos. Chem. Phys. 2008; 8: 5373-5391.

Brune WH, Baier BC, Thomas J, Ren X, Cohen RC, Pusede SE, et al. Ozone production chemistry in the presence of urban plumes. Faraday Discuss. 2016; 189: 161-189.

Cardelino C, Chameides W. An observation-based model for analyzing ozone precursor relationships in the urban atmosphere. Journal of the Air & Waste Management Association 1995; 45: 161-180.

Cazorla M, Brune W, Ren X, Lefer B. Direct measurement of ozone production rates in Houston in 2009 and comparison with two estimation methods. Atmos. Chem. Phys. 2012; 12: 1203-1212.

Cazorla M, Brune WH. Measurement of Ozone Production Sensor. Atmos. Meas. Tech. 2010; 3: 545-555.

Chen S, Wang H, Lu K, Zeng L, Hu M, Zhang Y. The trend of surface ozone in Beijing from 2013 to 2019: Indications of the persisting strong atmospheric oxidation capacity. Atmospheric Environment 2020; 242: 117801.

408

409 410

411 412

413 414

415 416 417

418 419

420 421

422 423 424

425

426 427

428 429 430

431 432

433 434

435

436 437

438 439 440

441 442 443

444 445 446

447 448 449

450 451 452

453 454 455

456 457 458

459 460

Cuesta J, Kanaya Y, Takigawa M, Dufour G, Eremenko M, Foret G, et al. Transboundary ozone pollution across East Asia: daily evolution and photochemical production analysed by IASI+GOME2 multispectral satellite observations and models. Atmos. Chem. Phys. 2018; 18: 9499-9525.

Ding AJ, Wang T, Thouret V, Cammas JP, Nédélec P. Tropospheric ozone climatology over Beijing: analysis of aircraft data from the MOZAIC program. Atmos, Chem. Phys. 2008;

Griffith SM, Hansen RF, Dusanter S, Michoud V, Gilman JB, Kuster WC, et al. Measurements of Hydroxyl and Hydroperoxy Radicals during CalNex-LA: Model Comparisons and Radical Budgets. J. Geophys. Res. 2016; 121: 4211-4232.

Guo S, Hu M, Zamora ML, Peng J, Shang D, Zheng J, et al. Elucidating severe urban haze formation in China. Proc. Natl. Acad. Sci. U.S.A. 2014; 111: 17373-8.

Huang RJ, Zhang Y, Bozzetti C, Ho KF, Cao JJ, Han Y, et al. High secondary aerosol contribution to particulate pollution during haze events in China. Nature 2014; 514: 218-22.

Kanaya Y, Cao R, Akimoto H, Fukuda M, Komazaki Y, Yokouchi Y, et al. Urban photochemistry in central Tokyo: 1. Observed and modeled OH and HO2 radical concentrations during the winter and summer of 2004. J. Geophys. Res. 2007; 112: 312.

Kanaya Y, Fukuda M, Akimoto H, Takegawa N, Komazaki Y, Yokouchi Y, et al. Urban photochemistry in central Tokyo: 2. Rates and regimes of oxidant (O3 + NO2) production. J. Geophys. Res. 2008; 113: D06301.

Kaser L, Patton EG, Pfister GG, Weinheimer AJ, Montzka DD, Flocke F, et al. The effect of entrainment through atmospheric boundary layer growth on observed and modeled surface ozone in the Colorado Front Range. Journal of Geophysical Research: Atmospheres 2017; 122: 6075-6093.

Kim S, VandenBoer TC, Young CJ, Riedel TP, Thornton JA, Swarthout B, et al. The primary and recycling sources of OH during the NACHTT-2011 campaign: HONO as an important OH primary source in the wintertime. J. Geophys. Res. 2014; 119: 6886-6896.

Kleinman LI, Daum PH, Lee YN, Nunnermacker LJ, Springston SR, Weinstein-Lloyd J, et al. Ozone production efficiency in an urban area. J. Geophys. Res. 2002; 107: 12.

Kley D, Geiss H, Mohnen VA. Tropospheric ozone at elevated sites and precursor emissions in the United States and Europe. Atmos. Environ. 1994; 28: 149-158.

Lei L, Zhou W, Chen C, He Y, Li ZJ, Sun JX, et al. Long-term characterization of aerosol chemistry in cold season from 2013 to 2020 in Beijing, China. Environmental Pollution 2021; 268.

Li K, Jacob DJ, Shen L, Lu X, De Smedt I, Liao H. Increases in surface ozone pollution in China from 2013 to 2019: anthropogenic and meteorological influences. Atmos. Chem. Phys. 2020; 20: 11423-11433.

Liu SC. Possible effects on fropospheric O 3 and OH due to No emissions. Geophys. Res. Lett. 1977; 4: 325-328.

Lu K, Fuchs H, Hofzumahaus A, Tan Z, Wang H, Zhang L, et al. Fast Photochemistry in Wintertime Haze: Consequences for Pollution Mitigation Strategies. Environmental Science & Technology 2019a.

Lu K, Zhang Y, Su H, Brauers T, Chou CC, Hofzumahaus A, et al. Oxidant (O3 + NO2) production processes and formation regimes in Beijing. Journal of Geophysical Research: Atmospheres 2010; 115: D07303.

Lu X, Zhang L, Chen Y, Zhou M, Zheng B, Li K, et al. Exploring 2016–2017 surface ozone pollution over China: source contributions and meteorological influences. Atmos. Chem. Phys. 2019b; 19: 8339-8361.

Ma X, Tan Z, Lu K, Yang X, Liu Y, Li S, et al. Winter photochemistry in Beijing: Observation and model simulation of OH and HO2 radicals at an urban site. Science of The Total Environment 2019: 685: 85-95.

Martinez M, Harder H, Kovacs TA, Simpas JB, Bassis J, Lesher R, et al. OH and HO2 concentrations, sources, and loss rates during the Southern Oxidants Study in Nashville, Tennessee, summer 1999. Journal of Geophysical Research-Atmospheres 2003; 108.

462

463 464

465 466

467 468 469

470

471 472

474 475

473

476 477 478

479 480

481 482

483 484 485

486 487 488

489 490 491

492 493 494

495 496 497

498 499 500

501

502 503 504

505 506 507

508 509

510 511 512

513 514

515 516

Michoud V, Kukui A, Camredon M, Colomb A, Borbon A, Miet K, et al. Radical budget analysis in a suburban European site during the MEGAPOLI summer field campaign. Atmos. Chem. Phys. 2012; 12: 11951-11974.

Mihelcic D, Holland F, Hofzumahaus A, Hoppe L, Konrad S, Müsgen P, et al. Peroxy radicals during BERLIOZ at Pabstthum: Measurements, radical budgets and ozone production. Journal of Geophysical Research: Atmospheres (1984–2012) 2003; 108.

Ren XR, van Duin D, Cazorla M, Chen S, Mao JQ, Zhang L, et al. Atmospheric oxidation chemistry and ozone production: Results from SHARP 2009 in Houston, Texas. J. Geophys. Res. 2013; 118: 5770-5780.

Riedel TP, Wagner NL, Dube WP, Middlebrook AM, Young CJ, Ozturk F, et al. Chlorine activation within urban or power plant plumes: Vertically resolved ClNO2 and Cl-2 measurements from a tall tower in a polluted continental setting. Journal of Geophysical Research-Atmospheres 2013; 118: 8702-8715.

Shirley TR, Brune WH, Ren X, Mao J, Lesher R, Cardenas B, et al. Atmospheric oxidation in the Mexico City Metropolitan Area (MCMA) during April 2003. Atmos. Chem. Phys. 2006; 6: 2753-2765.

Slater EJ, Whalley LK, Woodward-Massey R, Ye C, Lee JD, Squires F, et al. Elevated levels of OH observed in haze events during wintertime in central Beijing. Atmos. Chem. Phys. 2020; 20: 14847-14871.

Stein AF, Draxler RR, Rolph GD, Stunder BJB, Cohen MD, Ngan F. NOAA's HYSPLIT Atmospheric Transport and Dispersion Modeling System. Bulletin of the American Meteorological Society 2015; 96: 2059-2077.

Sun YL, Jiang Q, Wang ZF, Fu PQ, Li J, Yang T, et al. Investigation of the sources and evolution processes of severe haze pollution in Beijing in January 2013. Journal of Geophysical Research-Atmospheres 2014; 119: 4380-4398.

Tan Z, Fuchs H, Lu KD, Hofzumahaus A, Bohn B, Broch S, et al. Radical chemistry at a rural site (Wangdu) in the North China Plain: observation and model calculations of OH, HO2 and RO2 radicals. Atmospheric Chemistry and Physics 2017; 17: 663-690.

Tan Z, Lu K, Dong H, Hu M, Li X, Liu Y, et al. Explicit diagnosis of the local ozone production rate and the ozone-NOx-VOC sensitivities. Sci. Bull. 2018a; 63: 1067-1076.

Tan Z, Lu K, Hofzumahaus A, Fuchs H, Bohn B, Holland F, et al. Experimental budgets of OH, HO2, and RO2 radicals and implications for ozone formation in the Pearl River Delta in China 2014. Atmospheric Chemistry and Physics 2019; 19: 7129-7150.

Tan Z, Rohrer F, Lu K, Ma X, Bohn B, Broch S, et al. Wintertime photochemistry in Beijing: observations of ROx radical concentrations in the North China Plain during the BEST-ONE campaign. Atmos. Chem. Phys. 2018b; 18: 12391-12411.

Tan Z, Rohrer F, Lu K, Ma X, Bohn B, Broch S, et al. Wintertime photochemistry in Beijing: observations of ROx radical concentrations in the North China Plain during the BEST-ONE campaign. Atmospheric Chemistry and Physics 2018c; 18: 12391-12411.

Thornton JA, Wooldridge PJ, Cohen RC, Martinez M, Harder H, Brune WH, et al. Ozone production rates as a function of NOx abundances and HOx production rates in the Nashville urban plume. Journal of Geophysical Research-Atmospheres 2002; 107.

Wang HC, Lu KD, Chen XR, Zhu OD, Chen O, Guo S, et al, High N2O5 Concentrations Observed in Urban Beijing: Implications of a Large Nitrate Formation Pathway. Environ. Sci. Technol. Lett. 2017a; 4: 416-420.

Wang T, Ding A, Gao J, Wu WS. Strong ozone production in urban plumes from Beijing, China. Geophysical Research Letters 2006; 33.

Wang T, Xue L, Brimblecombe P, Lam YF, Li L, Zhang L. Ozone pollution in China: A review of concentrations, meteorological influences, chemical precursors, and effects. Sci Total Environ 2017b; 575: 1582-1596.

Wang W, Parrish DD, Li X, Shao M, Liu Y, Mo Z, et al. Exploring the drivers of the increased ozone production in Beijing in summertime during 2005–2016. Atmos. Chem. Phys. 2020; 20: 15617-15633.

Whalley LK, Slater EJ, Woodward-Massey R, Ye C, Lee JD, Squires F, et al. Evaluating the sensitivity of radical chemistry and ozone formation to ambient VOCs and NOx in Beijing. Atmos. Chem. Phys. Discuss. 2020; 2020: 1-41.

517	Whalley LK, Slater EJ, Woodward-Massey R, Ye CX, Lee JD, Squires F, et al.
518	Evaluating the sensitivity of radical chemistry and ozone formation to ambient VOCs and
519	NOx in Beijing. Atmospheric Chemistry and Physics 2021; 21: 2125-2147.
520	Whalley LK, Stone D, Dunmore R, Hamilton J, Hopkins JR, Lee JD, et al.
521	Understanding in situ ozone production in the summertime through radical observations and
522	modelling studies during the Clean air for London project (ClearfLo). Atmos. Chem. Phys.
523	2018; 18: 2547-2571.
524	Xue LK, Wang T, Gao J, Ding AJ, Zhou XH, Blake DR, et al. Ground-level ozone in
525	four Chinese cities: precursors, regional transport and heterogeneous processes. Atmos. Chem.
526	Phys. 2014; 14: 13175-13188.
527	Young CJ, Washenfelder RA, Roberts JM, Mielke LH, Osthoff HD, Tsai C, et al.
528	Vertically resolved measurements of nighttime radical reservoirs in Los Angeles and their
529	contribution to the urban radical budget. Environ Sci Technol 2012; 46: 10965-73.
530	Zhang Q, Yuan B, Shao M, Wang X, Lu S, Lu K, et al. Variations of ground-level O3
531	and its precursors in Beijing in summertime between 2005 and 2011. Atmospheric Chemistry
532	and Physics 2014; 14: 6089-6101.
533	